Journal of the Korean Society of Surveying, Geodesy, Photogrammetry and Cartography
Vol. 33, No. 6, 537-545, 2015
http://dx.doi.org/10.7848/ksgpc.2015.33.6.537

ISSN 1598-4850(Print)
ISSN 2288-260X(Online)
Original article

Retrieval and Analysis of Integrated Water Vapor from Precise GPS Data Processing at IEODO Ocean Research Station

Lee, Hungkyu[1] · Musa, Tajul Ariffin[2] · Choi, Yunsoo[3] · Yoon, Hasu[4] · Lee, Dong-In[5]

Abstract

This paper deals with the retrieval of integrated water vapor (IWV) from the zenith tropospheric delay estimated by precisely processing GPS observations at IEODO ocean research station in the East China Sea. A comparison of GPS-IWV with the radiosonde profiling from June and November in 2014 was made to confirm the method and the procedure, adopted for the IWV determination. A series of analysis of these IWV values was performed to capture characteristics of their seasonal and diurnal variations. Furthermore, the troposphere around the ocean research station during typhoon events was spatiotemporally analyzed by including thirteen GPS sites over the Korean Peninsula, indicating correlation between the typhoon location and the tropospheric density.

Keywords : GPS, Integrated Water Vapor, Tropospheric Delay, IEODO

1. Introduction

The Water vapor is one of the most critical elements in the Earth's atmosphere, since it plays a significant role in the atmosphere process. Also, its distribution contributes to the vertical stability of atmosphere and evolution of the storm system. Furthermore, the water vapor is closely related with that of cloud and rainfall, which directly or indirectly impacts on the numerical weather prediction modelling. The GPS METeorology (GPS/MET) has been successfully developed over the last two decades (Bevis, *et al*., 1992; Bevis, *et al*., 1994; Duan, *et al*., 1996; Jin and Xi, 2014). This technology basically enables to retrieve the integrated water vapor (IWV) from the zenith total tropospheric delay (ZTD) from the GPS measurements. Taking into account the density of liquid water, the IWV, expressed in kg/m^2, is equivalent to the total percipitable water in mm of liquid water.

Comparing to the traditional meteorological sensors, the GPS/MET has more benefits which make it possible to cost-effectively measure the IWV either in near real-time, or in post-mission mode with high temporal resolution and in all-weather conditions (Bevis, *et al*, 1992; Jin and Xi, 2014; Wang *et al*., 2013). The GPS/MET is also capable of delivering the water vapor estimates with competitive accuracy of microwave radiometer, radiosonde (RS) and

Received 2015. 11. 29, Revised 2015. 12. 14, Accepted 2015. 12. 22
1) Corresponding Author, Member, School of Civil, Environmental and Chemical Engineering, Changwon National University (E-mail: hkyulee@changwon.ac.kr)
2) Faculty of Geoinformation and Real Estate, Universiti Tecknologi Malaysia (E-mail: tajulariffin@utm.my)
3) Member, Department of Geoinformatics, University of Seoul (E-mail: choiys@uos.ac.kr)
4) Member, Department of Geoinformatics, University of Seoul (E-mail: hasu9@uos.ac.kr)
5) Department of Environmental Atmospheric Sciences, Pukyong National University (E-mail: leedi@pknu.ac.kr)

the very long baseline interferometry (VLBI) (Bevis, *et al*., 1992; Emardson, *et al*., 1998; Van Baelen, *et al*., 2005). Due to these factors, this technique has been mainly used for the short-term and the disastrous weather forecasting as an independent data source for data assimilation (Wang *et al*., 2013).

The Ieodo ocean research station (IORS), an offshore fixed plant structure, was constructed on the Scotra Rock in the East China Sea. The station has mainly supported scientific research activities on natural disaster and ocean environment, such as earthquakes, typhoons, and ocean climate changes. It equips with a great number of the state-of-art oceanic, environmental and meteorological sensors; hence, their observations are provided via internet in real-time for 24 hours a day. The IORS, an unmanned research station, has been remotely operated by Korea Hydrographic and Oceanographic Authority (KHOA). In 2009, the Global Navigation Satellite System (GNSS) station was set up on the roof deck at the station (hereafter IEOD) to support marine geodetic research activities. While a Trimble NetRS receiver and TRM 41249.00 antenna were initially installed, they have been later replaced by NetR9 and TRM 55971.00 in January 2013. The typhoons normally pass through the IORS before they arrive to the Korean Peninsula. Therefore, the GNSS station has recently drawn meteorologists' attention to use it as a meteorological sensor for numerical weather modelling during the severe weather event.

Those GPS measurements, obtained by IEOD from 2009 to 2014, have been precisely processed by using the Bernese 5.0 software to estimate the ZTD; the IWV has been retrieved if meteorological data was available. The GPS-estimated IWV has been compared with those of RS profiled in June and November of 2014 to validate the method and the procedure, which adopted for the IWV retrieval process. The temporal analysis was carried out to understand seasonal and diurnal variations of the IWV. Subsequently, the intensive spatiotemporal analysis on distributions of ZTD and IWV during two typhoon events was made over the East China Sea and the Korean Peninsula to observe the correlation of typhoon location and water vapor distributions. All the details of analyzed results are summarized in this paper with a view to maximize the role of IORS GPS station in the field of ocean atmospheric and meteorological researches.

2. Observation and Methodology

This section describes those GPS and RS observations and the methodology, which have used to retrieve the IWV from them in this research.

2.1 GPS

The IEOD station has been established on the roof deck of IORS in 2009 and operated continuously since then. However, it is noted that the general operational condition of station faces the harshness due to the limited electric power supply and internet connection. This is mainly due to the fact that few tens of sensors at IORS are operating together; therefore, the power supply is controlled by an automatic system with the list of sensor priority during its shortage. Unfortunately, a GPS receiver is not ranked in the top of list, but resulted in unavoidable power disconnection. Since the IEOD receiver is not connected to communication network, the observation files can be only backed up if staffs of the KHOA pay visit to IORS for maintenance purpose. Furthermore, the GPS data, which if stored in the internal memory, had to be overwritten, if the periodic backup is not possible due to the severe weather condition. Table 1 summarizes the number of days, when GPS data was backed up at IEOD during the period of 2009 to 2014. Note that the GPS measurements of 2010 and 2012 were not considered in the data processing due to their limitation.

Table 1. The number of days in which GPS data is available at IEOD

Year	2009	2010	2011	2012	2013	2014	Total
Number of Days	139	4	235	28	109	145	928
Data Available Rates (%)	53.7	1.1	64.4	7.8	30.0	74.0	42.4

Table 2. GPS data processing parameters for estimation of the zenith total path delay

Parameters		Description	Parameters		Description
Duration of Analysis		24 hours	Absolute Antenna Phase Correction		IGS08.ATX
Type of Orbit and ERP		IGS Final Products	Cutoff Elevation Angle		3°
Tidal Effects	Earth	IERS Convention 2000	ZTD Estimation	Mapping Function	Neill
	Ocean	FES2004		Horizontal Gradient	Estimated

The total 896 days of GPS observations have been processed by using the scientific GNSS data processing software (i.e., Bernese version 5.0) with application of processing parameter shown in Table 2, so as to estimate ZTD at one hour interval. The software provides several unique tools useful to handle a huge number of GPS measurements (Gendt, *et al*., 2007). For instance, the Bernese processing engine (BPE), adopted in this research, automatically processes GPS data according to predefined scripts. Since the double-differenced technique was utilized for ZTD estimation, those ten IGS (International GNSS Services) stations around the Northeast Asia region were included. In Fig. 1, GPS measurements of thirteen continuously operation reference stations (CORS) from the national geographic information institute of Korea (NGII) were included for the spatiotemporal analysis of ZTD and IWV around the East China Sea and Korean Peninsula during typhoons' passages. A selection of these NGII station was made with a consideration of computational burden as well as spacing between them about 40 to 50 km around southern part of the Korean Peninsular.

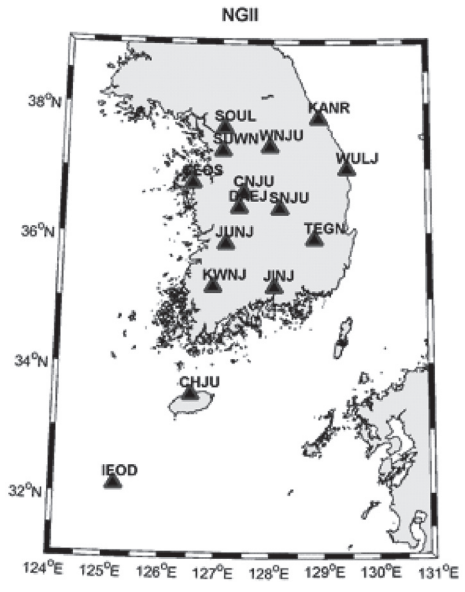

Fig. 1. A network of GPS sites included in precise data processing

For GPS-IWV retrieval, the zenith wet delay (ZWD) should be firstly obtained through subtracting the zenith hydrostatic delay (ZHD) from ZTD. Since the Saastamoinen model was adopted for this ZHD computation procedure (Saastamoinen, 1973), the IWV is retrieved from the ZWD by using following equations (Bevis, *et al*., 1992; Bevis, *et al*., 1994; Duan, *et al*., 1996):

$$IWV = \Pi \times ZWD \tag{1}$$

with:

$$\Pi = \frac{10^6}{R_v\left[\frac{k_3}{T_m} + k'_2\right]} \tag{2}$$

where R_v is the specific gas constant for water vapor, T_m is the weighted mean temperature of atmosphere (K), $k'_2 = k_2 - mk_1$, m is the ratio of the molar masses of water vapor and dry air (Davis *et al*., 1985). In this paper we use $k_1 = 77.604 K/mbar$, $k_2 = 64.79 mbar^{-1}$ and $k_3 = 3.776 \times 10^5 K/mbar$, respectively (Bevis, *et al*., 1992). Also, the Korean weighted mean temperature equation was used for T_m calculation (Song and Grejner-Brezinska, 2009).

2.2 Radiosonde (RS)

The total of 25 launches of RS was made at IORS in June and November of 2014. A Fig. 2 shows a setup of the RS trials

Table 3. Data and time of the radiosonde launching at IORS in 2014

Launching ID	Month-Day (Day of Years)	Time (UTC)	Launching ID	Month-Day (Day of Years)	Time (UTC)
1	06-24(175)	21:00	14	06-28 (179)	03:00
2	06-25 (176)	03:00	15		09:00
3		09:00	16		15:00
4		15:00	17		21:00
5		21:00	18	06-29 (180)	03:00
6	06-26 (177)	03:00	19	11-27 (331)	21:00
7		09:00	20	11-28 (332)	09:00
8		15:00	21	11-28 (332)	21:00
9		21:00	22	11-29 (333)	09:00
10	06-27 (178)	03:00	23	11-29 (333)	21:00
11		09:00	24	11-30 (334)	09:00
12		15:00	25	12-01 (335)	09:00
13		21:00			

for atmospheric sounding. Information of date and time of RS trials are tabulated in Table 3. For the experimental missions, DFM-09 radiosondes were flown into sky to profile those - the pressure, temperature, humidity, wind speed and direction in atmosphere at one second interval (e.g., see http://www.graw.de in more details). Using the RS measurements in temperature, humidity, pressure and dew-point temperature, the IWV can be computed by using the trapezoidal method as below (Li, *et al*., 2006):

$$IWV = \frac{1}{2\rho_v g_s}\sum_{i=1}^{n-1}(p_i - p_{i+1})(q_i - q_{i+1}) \quad (3)$$

where ρ_v is the partial pressure of water vapor, g_s is the gravity acceleration, and p_i and q_i is pressure and humidity at a certain surface pressure level, respectively. Hence, a value of the IWV is computed from one radiosonde profile. For the IWV computation, those nine pressure levels are integrated from surface pressure from 1,000 to 200hPa.

Fig. 2. View of radiosonde experiment at IORS in 2014

3. Retrieval and Comparison of IWV from GPS and Radiosonde

3.1 GPS-retrieved IWV

Those ZTD values at one hour interval have been estimated from GPS measurements of IEOD, NGII and IGS stations for 928 days. The Fig. 3 shows daily averaged ZTD values at IEOD from 2009 to 2014. The results of year 2010 and 2012 are not included in these graphs due to previously mentioned reason. Although 42% of the GPS measurements is available for six years, a seasonal variation from the estimated ZTD can be seen from the graphs. For example, the ZTD maximum is at the beginning of August, while the minimum is either the end of December, or the beginning of January. In addition, the ZTD values depict seasonal tendency increasing in spring but decreasing in autumn.

The IWV has been retrieved from the ZTD by using Eq. (1) with application of meteorological data. The Fig. 4 shows temporal variation of the IWV values at IEOD. While the

upper graph presents the hourly IWV, the lower shows error-bar consisting of daily average and standard deviation of the values. As presented in Fig. 3 (i.e., ZTD temporal variation), the water vapor changes at the station shows typical patterns of increasing during the summer and decreasing during the winter. Following to the results, it is possible to note that the diurnal and daily variation of summer (e.g., July and August) are relatively small, although the values are higher than others. However, the deviation is high the spring (i.e., May) and the autumn (i.e., October). The maximum IWV is 76.3 km/m^2 on 1st in August, whereas the minimum is 3.3 kg/m^2 on 15th in April.

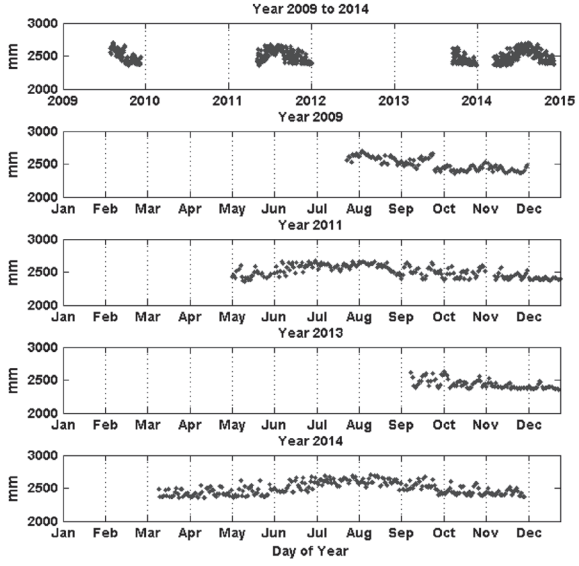

Fig. 3. Temporal variation of GPS-estimated ZTD at IEOD station from 2009 to 2014

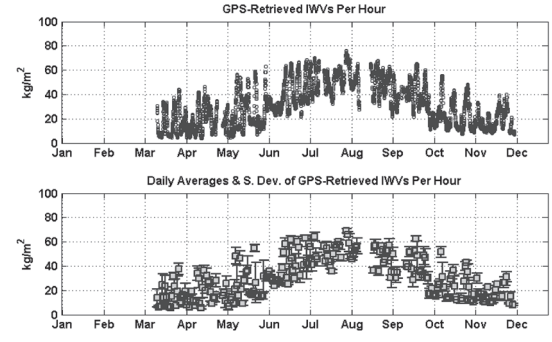

Fig. 4. Temporal variation of hourly GPS-estimated IWV at IEOD station in 2014

3.2 Comparison of IWV retrieved from GPS and radiosonde observations

By using Equation (3), those IWV values have been derived from twenty five launches in RS profiles (i.e., refer to Table 2). A Fig. 5 refers values of GPS- and RS-retrieved IWV from 24th to 29th in June of 2014, and 27th November to 1st December of 2014, respectively. While the GPS-IWV is plotted every hour in the figure, those of RS are plotted with respect to each launch of balloons.

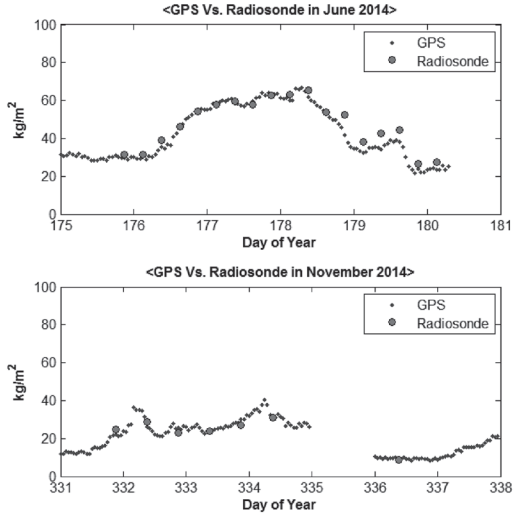

Fig. 5. Results of GPS- and RS-retrieved IWV values at IEOD in June and November 2014

The Fig. 6 provides a comparison of the IWV values that of estimated from GPS and RS observations. The top two graphs show the IWV differences between the techniques in June and November, whereas the bottom of those present the scaled differences by the RS-IWV, which can be considered as relative errors of GPS-IWV. In fact, the results at 20:00 on DoY (day of year) 178 and at 09:00 on 179 (i.e., RS launching ID 13 and 15 in Table 2) are excluded from the representation, as residuals are larger than $\pm 3\sigma$ (i.e., outliers). Since the number of two samples are not equal as well as limited, it is hard to rigorously compare these values through classifying them by the season. Nevertheless, following to the comparison, it can be observed from these results in the top graphs that the IWV differences (i.e., absolute errors of GPS-IWV) in the summer are larger

than those from the winter. Note that the root mean squares error (RMES) of the former is $\pm 2.7 kg/m^2$, while that of the latter is $\pm 2.1 kg/m^2$. This would be attributed from the fact that the amount of water vapor in troposphere is relatively large in the summer, but the humidity is usually low during winter season. In order to take account into this effect, the differences are scaled by the RS-IWV, and plotted in the bottom graphs of Fig. 6, which tells that the relative errors of the GPS-IWV of two samples are almost identical. A Fig. 7 illustrates distributions of correlations between the IWV from those GPS and RS measurements that demonstrates the strong linear correlations with coefficient in order of 0.991 and 0.949. However, those values of slope and intercept of the linear regression in the winter are 0.950 and 1.123; those are closer to unity compared to summer (i.e., 1.071 and –5.406). Such a result indicates that the GPS-retrieved IWV in June are slightly biased from those of RS.

The IWV deviation of two techniques would be induced by sensor measurement errors and/or algorithm's uncertainties, used for the IWV retrieval process. However, the magnitude of deviation in this study is slightly larger than other cases, including Van Baelen *et al.* (2005) and Sohn *et al.* (2012). In order to figure out a potential source of the deviation,

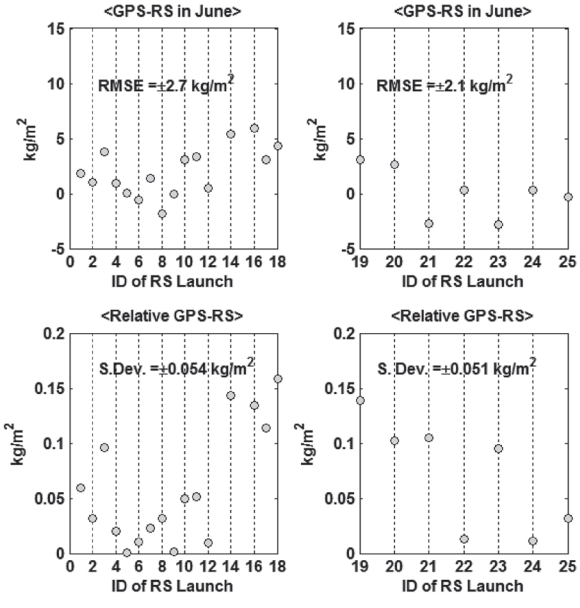

Fig. 6. Differences between GPS- and RS-retrieved IWV in June and November

those separated distances between IEOD and RS balloons at about 11km altitude are calculated on the reference ellipsoid (e.g., GRS80) and given in Fig. 8. In the distances range from 22.5km to 57.8km, the radiosonde does not appropriately profile the troposphere along the vertical line, but further investigations should be carried out to confirm the error source.

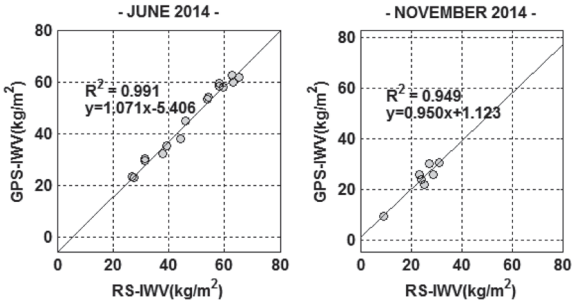

Fig. 7. Correlation between GPS- and RS-retrieved IWV in June and November

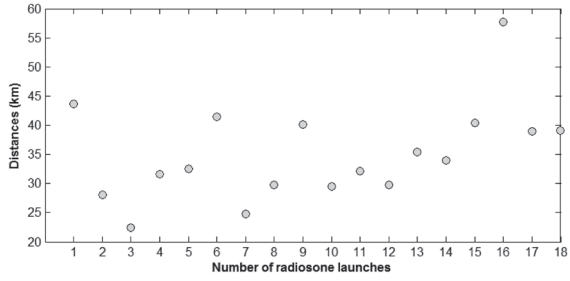

Fig. 8. Separations between IEOD and radiosonde balloons at altitude 11km

4. Some Analysis of GPS–derived Troposphere at IEODO

4.1. Diurnal variation

Since the atmospheric water vapor frequently changes with respect to local environment and time, it is difficult to derive features of temporal variation on a specific day. To this end, the diurnal variation in this study has been obtained by averaging one hour interval IWV over a month. The Fig. 9 illustrates the variation in May, July, September and November in 2014. The changes in May indicates an interesting patten that the IWV gradually increases from

the midnight to noon, whereas this trend goes into reverse from noon to midnight. The maximum range and deviation of variations are also observed in May. The results of September represent the lowest variation within a day, although the IWV values are larger than those of May. It is of interest to look into results of July that the IWV values are pretty stable during daytime, if they are compared with those of evening and night. Even if the variation of November is larger than those of July and September, its absolute magnitude is the smallest among them. As aforementioned in section 2.1, it should be noted that these analyses had a limitation of missing the IWV computation few days of GPS data in each corresponding month due to its availability. For this reason, further analysis with more abundant data is highly required to derive more reliable and scientifical characteristics of the diurnal variation at the IORS.

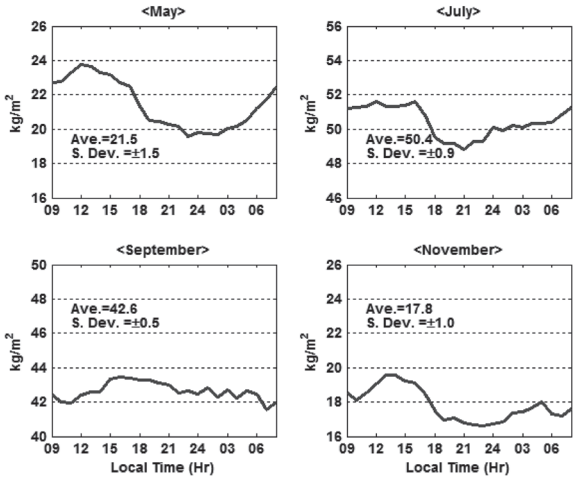

Fig. 9. Averaged diurnal variation of IWV in 2014

4.2 Spatiotemporal variation during typhoon events

A typhoon is a meteorological phenomenon which brings heavy rainfall and strong wind, which can be considered as one of the most devastating natural disasters in the northeast Asia region, especially in Korea. It is well known that understanding distribution of water vapor in atmosphere during typhoon passage is critical, since the quantity is the main source of precipitation and a dominant constituent of energy resources is related to typhoon dynamics. By considering geographical location of IORS laying a typhoon entrance to Korean Peninsula (see, e.g., Fig. 1), the GPS-retrieved IWV has a possibility in contribution on improving typhoon forecast in future.

Those preliminary attempts have been made here to spatiotemporally analyze the GPS-ZTD during the typhoon Maeri passage in 2013, and the GPS-IWV during the Neguri in 2014, respectively. The ZTD was analyzed during the typhoon Maeri event, instead of IWV, because meteorological data at IORS was not available. All the values were calculated one hour interval for IEOD as well as 13 NGII stations as seen in Fig. 1. Meteorological data for IWV computation at the NGII station has been

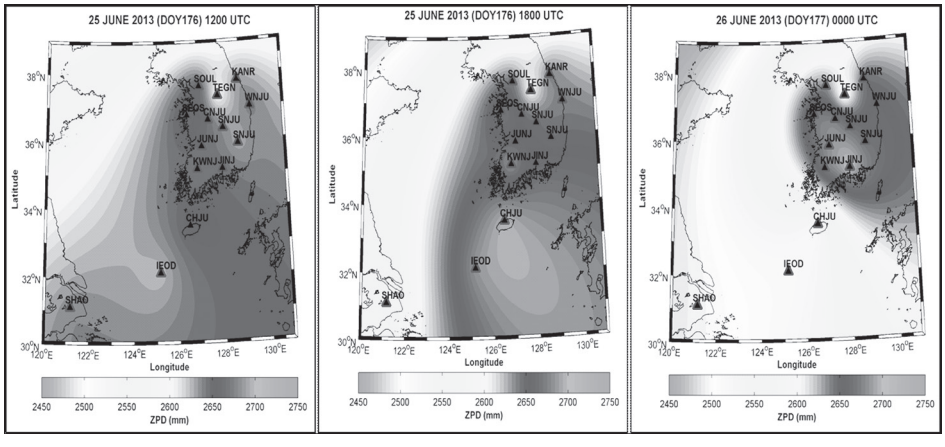

Fig. 10. Spatiotemporal variation of ZTD during typhoon Meari's passage

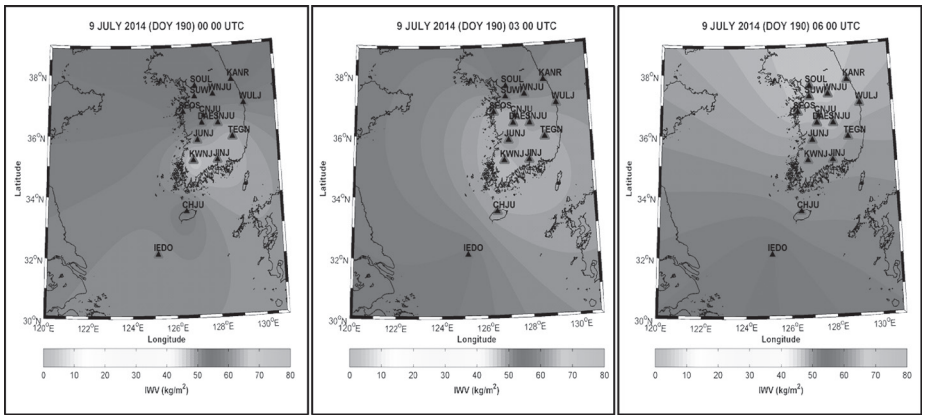

Fig. 11. Spatiotemporal variation of IWV during typhoon Neguri's passag

obtained from NNDC Climate Data Online (http://www7.ncdc.noaa.gov/CDO/cdo). While the Fig. 10 presents the spatial distribution of ZTD for 6 hours before and after the Meari's passage near the IORS, the Fig. 11 shows the spatial variation of IWV before and after the typhoon Neguri event in 2014. In fact, these plots are interpolated from the hourly GPS-estimates at 14 sites by the Kriging technique. The ZTD distribution in Fig. 10 indicates high magnitude before and during the passage near IORS, but these values get decreased after the event. On the other hand, pattern of the IWV variation for the Neguri is slightly different from that of the Meari. That is, the IWV does not get decreased even after the event. This should be attributed from fact that the typhoon courses deviate after passing IEOD in which the Meari moved northward to the Yellow Sea whereas the Neguri recurved northeast into the Japanese Archipelago.

5. Concluding Remarks

This research has been dealt with the estimation and analysis of integrated water vapor in atmosphere from GPS measurements at the IORS GNSS station in the East China Sea. The total of 928 days of GPS observations were processed to estimate the 1-h interval ZTDs at IORS and NGII stations. This was followed by retrieving IWV from the GPS-ZTD and RS measurements, if meteorological data was available to be used.

A series of intensive analysis has been subsequently carried out to capture features of GPS-IWV distribution around IORS. A comparison of the IWV from GPS and RS has revealed that two results were agreed within few kg/m^2 level with the strong linear correlation. In addition, the IWV deviation in summer was larger than that of winter, and according to linear regression, the GPS-IWV in June was biased from the RS-IWV. The temporal variations of IWV at IEOD had typical patterns, such of the IWV values and frequency of the variation increasing in the summer but decreasing in the winter. A diurnal analysis of the IWV indicated that the variation maximum appeared in May, whereas the minimum was in September; except for September the diurnal peaks exhibiting around noon, and the least at around midnight. Finally, the spatiotemporal analysis of IWV around the East China Seas showed the high magnitude of the meteorological element before and during the typhoon's passage, but the IWV decreased soon after the event. Therefore, it was possible to conclude in that the IWV distribution was correlated with the typhoon's location.

Acknowledgment

This research has been financially supported by the National Research Foundation of Korea (NRF-2014R1A1A2056133) and Korea Hydrographic and Oceanographic Administration. The authors would like to acknowledge the National Geographical Information

Institute (NGII) for providing GNSS data used in this research. Parts of this manuscript are an extension of a paper presented at 2015 International Symposium on GNSS, Kyoto, Japan, 16-19 November, 2015.

References

Bevis, M., Businger, S., and Chiswell, S. (1994), GPS meteorology: mapping zenith wet delays onto precipitable water, *Journal of Applied Meteorology*, Vol. 33, pp. 379-386.

Bevis, M., Businger, S., Herring, T.A., Rocken, C., Anthes, R.A., and Ware, R.H. (1992), GPS meteorology: remote sensing of atmospheric water vapor using the global positioning system, *Journal of Geophysical Research*, Vol. 97, No. D14, pp. 15787-15801.

Davis, J.H., Herring, T.A., Shapiro, I., Rogers, A., and Elgered, G. (1985), Geodesy by radio interferometry effects of atmospheric modeling errors on estimates of baseline length, *Radio Science*, Vol. 20, No. 6, pp. 1593-1607.

Duan, J., Bevis, M., Fang, P., Bock, Y., Chiswell, S., Businger, S., Rocken, C., Solheim, F., Hove, T.V., Ware, R., McClusky, S., Herring, T.A., and King, R.W. (1996), GPS meteorology: direct estimation of the absolute value of percipitable water, *Journal of Applied Meteorology*, Vol. 35, pp. 830-837.

Emardson, T.R., Elegered, G., and Johansson, J.M. (1998), Three months of continuous monitoring of atmospheric water vapor with a network of GPS receivers, *Journal of Geophysical Research*, Vol. 103, pp. 1807-1820.

Gendt, G. , Dach, R., Hugentobler, U., Fridez, P., and Meindl, M. (2007), *Bernese GPS Software Version 5.0 Manual*, Astronomical Institute, University of Bern, Swaziland, 612p.

Jin, S. and Xi, F. (2014), *GNSS Remote Sensing–Theory and Applications*, Springer Dordrecht Heidelberg New York London, 276p.

Li, G., Huang, D., Liu, B., and Chen, J. (2006), Experiment on driving precipitable water vapor from ground-based GPS network in Chengdu plain, *Geo-spatial Information Science of Wuhan University*, Vol. 10, No. 3, pp. 1086-1089.

Saastamoinen, J. (1973), Contribution to the theory of atmospheric refraction, *Bulletin Geodesique*, Vol. 107, pp. 13-34.

Sohn, D.H., Park, K.D., Won, J., Cho, J., and Roh, K.M. (2012), Comparison of the characteristics of precipitable water vapor measured by global positioning system and microwave radiometer, *Journal of Astronomy and Space Sciences*, Vol. 29, No. 1, pp. 1-12.

Song, D.S. and Grejner-Brzezinska, D.A. (2009), Remote sensing of atmospheric water vapor variation from GPS measurements during a severe weather event, *Earth Planets Space*, Vol. 61, pp. 1117-1125.

Van Baelen, J., Jean-Pierre, A., and Alain D. (2005), Comparison of near-real time estimates of integrated water vapor derived with GPS, radiosondes, and microwave radiometer, *Journal of Atmospheric and Oceanic Technology*, Vol. 22, No. 2, pp. 201-210.

Wang, H., Wei, M., Li, G., Zhou, S., and Zeng, Q. (2013), Analysis of precipitable water vapor from GPS measurements in Chengdu region: distribution and evolution characteristics in autumn, *Advances in Space Research*, Vol. 52, pp. 656-667.